

**Nonlinear transparency window for ultraintense femtosecond laser pulses in the atmosphere**Nikolay A. Panov,<sup>1,2,3,4</sup> Daniil E. Shipilo,<sup>1,3,4</sup> Alexander M. Saletsky,<sup>1</sup> Weiwei Liu,<sup>5</sup>  
Pavel G. Polynkin,<sup>6</sup> and Olga G. Kosareva<sup>1,3,4,5,\*</sup><sup>1</sup>*Physics Faculty, M. V. Lomonosov Moscow State University, 1/2 Leninskie Gori, Moscow 119991, Russia*<sup>2</sup>*International Laser Center, M. V. Lomonosov Moscow State University, 1/62 Leninskie Gori, Moscow 119991, Russia*<sup>3</sup>*P. N. Lebedev Physical Institute of Russian Academy of Sciences, 53 Leninskiy Prospekt, Moscow 119991, Russia*<sup>4</sup>*Institute of Spectroscopy of Russian Academy of Sciences, 5 Fizicheskaya Street, Troitsk, Moscow 108840, Russia*<sup>5</sup>*Institute of Modern Optics, Nankai University, Tianjin 300350, China*<sup>6</sup>*College of Optical Sciences, University of Arizona, Tucson, Arizona 85721, USA*

(Received 10 April 2019; published 21 August 2019)

We have found the optimum range of driver wavelengths for mid-infrared ultraintense femtosecond pulses undergoing filamentation in atmospheric air. This wavelength range between 3.1 and 3.5  $\mu\text{m}$  forms a nonlinear transparency window identified through a diligent scan of pulse central wavelengths in the range 2.2–4.7  $\mu\text{m}$  with a best resolution of 5 nm. Each of 123 wavelengths scanned corresponds to the solution of the full three-dimensional + time pulse propagation and filamentation problem on a 7–19 m path in air. Due to the discovered universal asymmetric character of the nonlinearly enhanced linear absorption in the vicinity of atmospheric molecular band, the optimum driver wavelength belongs to the long-wavelength side of the band.

DOI: [10.1103/PhysRevA.100.023832](https://doi.org/10.1103/PhysRevA.100.023832)**I. INTRODUCTION**

Ten years after the Nobel-Prize-winning chirped pulse amplification technique was first implemented [1], the unique regime of long-range femtosecond pulse propagation without beam divergence was discovered [2] and studied with Ti:Sapphire laser systems centered at  $\sim 800$  nm with typical duration of 35–200 fs and power of  $10^{10}$ – $10^{13}$  W [3–8]. In this filamentation regime the free electrons due to photoionization prevent the self-focusing collapse in air and support  $\sim 100$ - $\mu\text{m}$ -diameter plasma and light strings with a loss of not more than 10% along hundreds of meters [9,10]. An atmospheric transparency window [11] in the visible range ensures the lossless propagation of the supercontinuum blue wing in the course of backward propagation after reflection from the cloud [12–14].

The fingerprints of atmospheric molecular pollutants are in the mid- and far-infrared range [11]. The supercontinuum of an 800-nm filament can span to 12  $\mu\text{m}$ , but its spectral intensity drops by six orders of magnitude at 4  $\mu\text{m}$  and by nine orders at 10  $\mu\text{m}$  [15]. The use of a longer-wavelength driver (mid- or far-infrared) will boost the spectral intensity of the supercontinuum at these wavelengths by several orders of magnitude [8] and increase the sensitivity of femtosecond lidars [12]. Compared to far-infrared drivers, the mid-infrared (MIR) ones are amplified in solid-state media and thus have the shorter pulse duration, better pulse shape, and much lower energy for filament formation (tens of millijoules [16] as compared to several joules [17]). Enhancement of the mid-to-far-infrared wing of the supercontinuum of MIR filaments as well as the moderate pulse energy needed to form a filament

constitute a decisive advantage of a MIR laser as compared to a source in the visible, near-infrared, or far-infrared range. So, the key application we target in our studies is a femtosecond lidar in the MIR part of the spectrum, including the potential possibility of its mobile version, as was done with an 800-nm laser system [14].

MIR frontiers of femtosecond laser manufacturing exploit the optima in parametric [18] and chirped pulse amplification laser systems. Only a few existing laser setups exceed the critical power for self-focusing  $P_{\text{cr}}$  in the mid- and far-infrared range: at 2.1  $\mu\text{m}$  [19], 3.3–3.9  $\mu\text{m}$  [20], 3.3  $\mu\text{m}$  [21], 3.9  $\mu\text{m}$  [8,16], and 10.6  $\mu\text{m}$  [17]. With the MIR central wavelength, the conversion efficiency to the supercontinuum increases due to weak dispersion. With propagation the distinctly pronounced harmonics up to the 15th [19,22,23] introduce strong spectral intensity modulation smoothed over by the supercontinuum [24,25]. The Stokes side of the continuum reveals a robust well-separated hump [26–29], which continuously downshifts its central frequency and consumes up to ten percent of the pulse energy [27,30,31] with propagation.

A new mechanism of losses has been encountered for high-power MIR femtosecond pulses propagating in air. Although the pulse central wavelength is detuned from atmospheric absorption lines, the supercontinuum of this pulse spans across absorption bands of atmospheric compounds. As more energy is transferred to the supercontinuum, a larger fraction of the initial pulse energy is absorbed. This nonlinearly enhanced linear absorption (NELA) [25] has been observed with 2.1- $\mu\text{m}$  [19] and 3.9- $\mu\text{m}$  [16] drivers. Therefore, to use the beneficial properties of the MIR pulse supercontinuum for remote sensing, one has to center a femtosecond pump pulse at a wavelength avoiding both direct and nonlinearly enhanced absorption. The transparency windows were established for

\*kosareva@physics.msu.ru

low-power radiation [11]. For the higher-power case only three MIR central wavelengths of 2  $\mu\text{m}$  [32,33], 3.9  $\mu\text{m}$  [8,24,34], and  $\sim 10$   $\mu\text{m}$  [35–37] are being diligently discussed in the literature.

In this work we suggest a generalized approach for identification of the optimum laser wavelength for supercontinuum remote sensing applications through the calculation of the actual losses experienced by an ultraintense femtosecond pulse with a central wavelength in the range 2.2–4.7  $\mu\text{m}$ . The pulse central wavelength was scanned numerically in the same geometry of propagation with steps of 5–25 nm. Through this scan we identified the *nonlinear* transparency window for ultraintense femtosecond pulse in the atmosphere, which spans from 3.1 to 3.5  $\mu\text{m}$  and is half as wide as the window for low-energy femtosecond pulses (3.0–3.9  $\mu\text{m}$ ). Formation of the Stokes hump explains narrowing of the nonlinear transparency window for the filamenting pulse. The long-wavelength boundary of this window shrinks to accommodate this spectral hump. We elucidate the contribution of the resonant and nonresonant molecular absorption as well as the ionization loss on the 7–19-m propagation path. The newly found nonlinear transparency window manifests the region where the long plasma channel can be obtained and almost all the losses are associated with the plasma formation. This window will facilitate the search for the optimum driver wavelength for remote applications of the filament supercontinuum.

## II. MODEL

Our solver [25] for the near- and mid-infrared single filamentation study has been extended to take into account all types of air absorption relevant to ultraintense femtosecond pulse propagation. In addition to the resonant absorption [11] and ionization loss we included nonresonant absorption due to rotational excitations in  $\text{O}_2$  and  $\text{N}_2$  molecules. The solver is based on the forward Maxwell equation (FME) [38,39] for the time-domain Fourier harmonics  $\hat{E}(\omega, r, z)$  of the electric field  $E(t, r, z)$ :

$$\frac{\partial \hat{E}(\omega)}{\partial z} = -i \left( k(\omega) + \frac{\Delta_{\perp}}{2k(\omega)} \right) \hat{E}(\omega) - \frac{2\pi}{c} \hat{J}(\omega), \quad (1)$$

where  $\Delta_{\perp} = r^{-1} \partial / \partial r (r \partial / \partial r)$ ,  $r$  is the transverse coordinate,  $z$  is the propagation distance, and  $c$  is the speed of light in vacuum.

The first term at the right-hand side of Eq. (1) describes diffraction, dispersion, and resonant absorption through the complex-valued wave number  $k(\omega) = \omega[n'(\omega) + in''(\omega)]/c$ . The absorption  $n''(\omega)$  and refractive  $n'(\omega)$  indices are connected through the Kramers-Krönig relations [25]:

$$n'(\omega) = 1 + A + B\omega^2 + \mathcal{F}[\text{sgn}(t)\mathcal{F}^{-1}[in''(\omega)]]. \quad (2)$$

Here  $\mathcal{F}$  and  $\mathcal{F}^{-1}$  are the operators of direct and inverse Fourier transform respectively; constants  $A = 1.993 \times 10^{-4}$  and  $B = 0.558 \text{ as}^2$  determine the Cauchy equation. The dependence  $n''(\omega)$  in the range 1.2–20  $\mu\text{m}$  is approximated to our numerical grid using the data [40].

The nonlinear current is  $J(t) = J_{\text{free}} + J_{\text{abs}} + \partial P_{\text{inst}} / \partial t + \partial P_{\text{rot}} / \partial t$ , where  $J_{\text{free}}(t)$  and  $J_{\text{abs}}(t)$  are the free electron and absorption currents, respectively, and  $P_{\text{inst}}(t)$  is the third-order

instantaneous polarization of bound electrons. The excitation of rotational levels of  $\text{O}_2$  and  $\text{N}_2$  leads to delayed nonlinear response [41–43]:

$$P_{\text{rot}} = \chi_{\text{rot}}^{(3)} E(t) \int_{-\infty}^t K(t-t') E^2(t') dt', \quad (3)$$

where

$$K(t) = \sum_l e^{-W_l/T} [1 - e^{-\hbar\omega_{l,l+2}/T}] \sin \omega_{l,l+2} t, \quad (4)$$

the third-order susceptibility  $\chi_{\text{rot}}^{(3)}$  corresponds to the Kerr coefficient  $n_2 = 10^{-19} \text{ cm}^2/\text{W}$  [44],  $\hbar$  is Planck's constant, the temperature  $T = 290 \text{ K}$ ,  $W_l \propto l(l+1)$  is the energy of the  $l$ th rotational level, and  $\omega_{l,l+2} = (W_{l+2} - W_l)/\hbar$ . The summation in (4) is performed over the levels  $l$  up to 100, i.e., up to the rotational energy of 1.2 eV for an  $\text{O}_2$  molecule. At the room temperature  $l \approx 15$  rotational levels are excited. Equations (3) and (4) were solved independently for  $\text{N}_2$  and  $\text{O}_2$ . The current  $\partial P_{\text{rot}} / \partial t$  oscillates at the optical frequency and ensures both the nonlinear absorption and refraction.

The initial pulse was linearly polarized and Gaussian in space and time, with a duration of 96 fs at  $e^{-1}$  intensity level (80 fs FWHM) and an energy of 34 mJ for all the central wavelengths  $\lambda_0$  studied (2.2–4.7  $\mu\text{m}$ ). The peak power of this pulse corresponds to  $\sim 4P_{\text{cr}}$  in the 2.7- $\mu\text{m}$  band center and ensures single filamentation through all the range of  $\lambda_0$ . The beam diameter was set to be 4 mm so that the filament could be initiated and terminated within a 7–19 m path in close-to-reality conditions [16]. The atmospheric parameters are temperature 290 K, humidity 10%, and  $\text{CO}_2$  density 0.04%. These parameters were fixed so as to ensure standardized conditions for our transmission “experiment.”

We intentionally use a fixed pulse duration (and spectral width  $\Delta\omega$  in the frequency domain) as well as a fixed energy for all the wavelengths studied. Our parameters are within the up-to-date experimental possibilities:  $\sim 30$ -mJ,  $\sim 100$ -fs pulses are available on both edges of a 3–4  $\mu\text{m}$  interval [16,21]. In principle, the simulations with the fixed pulse power  $P$  excess over the critical power for self-focusing  $P_{\text{cr}}$  (so that  $P \propto \lambda_0^2$ ) and fixed pulse duration would lead us to the same nonlinear transparency window 3.1–3.5  $\mu\text{m}$  (within the window critical power differs by  $\sim 25\%$  only), but the simulated pulse energies would grow to about 100 mJ at 4.5  $\mu\text{m}$ , far beyond the state of the art of femtosecond lasers in this range. Any manipulation of the initial pulse duration (e.g., if one fixes the number of optical cycles in the input pulse) results in the variation of the initial pulse spectrum with the central wavelength and, therefore, in the spectrum of the supercontinuum. The comparison of absorption of such pulses with different wavelengths  $\lambda_0$  and the  $\Delta\omega$  depending on this  $\lambda_0$  seems to be less useful for researchers.

The spatio-temporal grid of our FME solver contains  $2^{16}$  equidistant temporal and 1500 nonequidistant spatial nodes with resolutions of 146 as and 2  $\mu\text{m}$ , respectively. The frequency resolution is 100 GHz. The average single-run duration on our workstation with four Intel Xeon E7-4870 processors was 3 days using 16-thread parallelization. We did 123 basic runs (including self-focusing, plasma production,

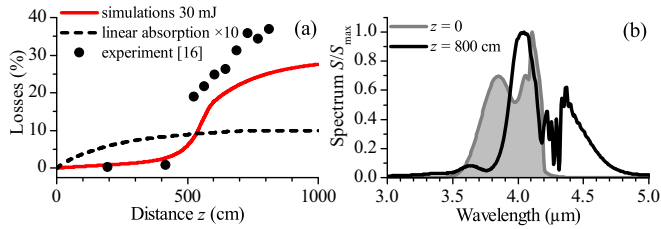


FIG. 1. (a) Accumulation of the fraction of the absorbed energy with propagation distance in the experiment in air [16] (dots) and our simulations (red solid curve) in the conditions of the experiment [16]. (b) The spectrum of the simulated pulse before (filled gray line) and after filamentation in air in the conditions of the experiment [16].

delayed rotational Raman response of  $N_2$  and  $O_2$  molecules, and resonant vibrational absorption) for a 34-mJ pulse with  $\lambda_0 = 2.2\text{--}4.7\ \mu\text{m}$ . The complementary runs were done with exactly the same pulse parameters as the basic ones, but we switched off either the Raman response (59 runs with  $\chi_{\text{rot}}^{(3)} = 0$ ) or the resonant absorption (4 runs with  $n'' = 0$ ). 123 special runs were performed with an energy of 0.1 mJ to avoid self-focusing and ionization while preserving resonant absorption. Further on we will refer to these runs as “full nonlinear problem,” “no Raman,” “no lines,” and “linear regime,” respectively.

### III. NONLINEAR TRANSPARENCY WINDOW IN MID-INFRARED

Experimental data on 3.9- $\mu\text{m}$ , 90-fs, 30-mJ pulse propagation along the 8-m laboratory path in air demonstrate 36% loss of the initial energy within the filament [16]. We benchmarked our model and solver against this experimental data by introducing the initial pulse parameters from Ref. [16] including the pulse spectrum with two maxima at 3.9 and 4.1  $\mu\text{m}$  (cf. filled spectrum in Fig. 1(b) and in Fig. 2 of Ref. [16]) as well as  $\text{CO}_2$  density of 0.06%. Both in the experiment and in the simulations the losses along the 8-m path are high: 36% and 25%, respectively [Fig. 1(a)]. These losses grow along the filament due to NELA. For the initial pulse energy of 0.1 mJ in the simulations we get 1% energy loss along the same path.

Near- to mid-infrared femtosecond pulse nonlinear transformation along the extended path in air has a distinct feature of self-shifted robust light bullet formation in the Stokes wing of the supercontinuum [16,27,30,31]. Since the essential amount of the initial pulse energy is transferred to the Stokes side of the spectrum, the location of the Stokes hump relative to the absorption band will affect the pulse energy losses, i.e., the actual nonlinear transparency of air. We demonstrate this with the example of the pulses centered at three selected representative wavelengths in Fig. 2(a), where the shaded areas show the input spectra and solid lines indicate the spectra after the filament termination. The left spectrum in Fig. 2(a) is initially centered exactly in the absorption band of  $\text{H}_2\text{O}$  and  $\text{CO}_2$  and loses more than one third of energy (36.6%). However, its Stokes hump escapes the absorption region and propagates up to  $z = 9\ \text{m}$  at least.

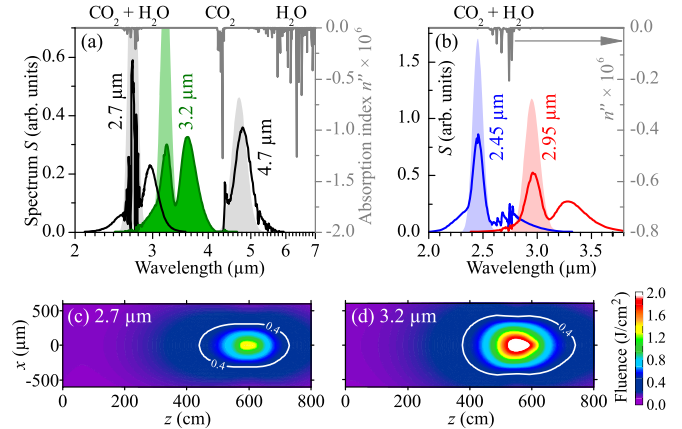


FIG. 2. (a,b) Spectra of MIR pulses at propagation end (solid lines) and start (shaded areas behind) for a set of initial central wavelengths. The gray line at the top is the absorption index (right axis). (c,d) Fluence channels for the pulses with the initial central wavelengths of 2.7 and 3.2  $\mu\text{m}$ .

The longer-wavelength pulse [right spectrum in Fig. 2(a),  $\lambda_0 = 4.7\ \mu\text{m}$ ] centered in between the absorption bands experiences severe absorption from both anti-Stokes and Stokes sides, and only the radiation at the fundamental wavelength is transmitted successfully. Hence, for this example the advantage of the MIR supercontinuum needed for remote sensing is almost lost.

The most confident propagation is attained for the pulse with the central wavelength  $\lambda_0 = 3.2\ \mu\text{m}$ . For this  $\lambda_0$  the broad continuum formation is accompanied by moderate 11% losses along the 19-m path [green filled spectrum in Fig. 2(a)]. Fluence distribution in the filament supports a value above 0.4  $\text{J}/\text{cm}^2$  in the transverse section with 0.8 mm in diameter and along 3 m in the propagation direction [Fig. 2(d)]. In contrast, an exhausted filament is formed at  $\lambda_0 = 2.7\ \mu\text{m}$  [Fig. 2(c)].

The formation of the Stokes hump is the characteristic feature for all spectra shown in Fig. 2(a), while the anti-Stokes wing is less pronounced. As the absorbed energy is proportional to the spectral power density overlapping the band, the short- and long-wavelength placement of the pulse central wavelength relative to the band gives notably different losses; see Fig. 2(b): the long-wavelength side is preferable for loss minimization.

We search for the central wavelength  $\lambda_0$  of MIR femtosecond pulses within the range 2.2–4.7  $\mu\text{m}$ , for which the energy loss after filamentation,  $\delta_{\text{full}}$  (“full nonlinear problem”), in air takes the minimum value (Fig. 3). The wavelength range where the absorption in the “linear regime”  $\delta_{\text{lin}}(\lambda_0) \leq 1\%$  is the transparency window for the low energy pulse. It spans from 3.0 to 3.9  $\mu\text{m}$  [Fig. 3(a)]. Note that the gap between its boundaries and absorption bands is  $\sim 300\ \text{nm}$ , i.e., about the spectral width of our  $\sim 100$ -fs pulse.

For the quantitative characterization of the nonlinear transparency window we introduce the difference  $\Delta(\lambda_0) = \delta_{\text{full}}(\lambda_0) - \delta_{\text{lin}}(\lambda_0)$  [Fig. 3(b)]. The physical meaning of the difference  $\Delta$  is the excess of the full loss at the end of the filament  $\delta_{\text{full}}$  over the loss for the low energy pulse  $\delta_{\text{lin}}$  defined by atmospheric constituents.

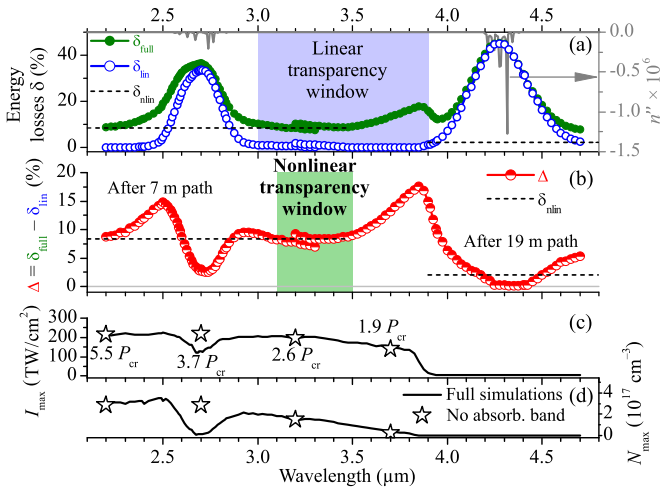


FIG. 3. Results of the simulations with the pulse central wavelength scanned from 2.2 to 4.7  $\mu\text{m}$ : (a) net losses over the whole propagation path [7 m (19 m)] for  $\lambda_0$  less (greater) than 3.4  $\mu\text{m}$ ] for the cases of (filled circles) “full nonlinear problem”  $\delta_{\text{full}}$ , (open circles) “linear regime”  $\delta_{\text{lin}}$ , and (dotted line) “no lines” propagation  $\delta_{\text{nlin}}$ ; the gray line is the linear absorption index profile  $n''$ ; (b) difference in net absorption between “full model” and “linear regime”; the dotted line is the same as in (a); (c) peak intensity and (d) peak plasma density over the whole propagation path; stars are the same quantities for “no lines” propagation.

Within the range 3.1–3.5  $\mu\text{m}$  the full loss in the filament is equal to the sum of the ionization and nonresonant Raman losses, and coincides with the ones in “no lines” simulations  $\delta_{\text{nlin}} \approx \Delta$  [Fig. 3(b), circles and dashed line within the green rectangle]. So, the range 3.1–3.5  $\mu\text{m}$  forms a nonlinear transparency window in the atmosphere. Outside this range there is natural domination of the resonant direct ( $\Delta < \delta_{\text{nlin}}$ ) or nonlinearly enhanced ( $\Delta > \delta_{\text{nlin}}$ ) absorption in the bands at 2.7 and 4.3  $\mu\text{m}$ .

The pragmatic advantage of the diligent scan over the MIR pulse central wavelength is identification of the nonlinearly enhanced linear absorption (NELA) efficiency maxima on the short-wavelength sides of both 2.7 and 4.3  $\mu\text{m}$  bands: 2.5 and 3.85  $\mu\text{m}$ , respectively [Fig. 3(b)]. The nonlinearly enhanced contribution of both bands to the overall pulse absorption constitutes  $\sim 10\%$ .

The nonlinearly enhanced absorption in the 2.7- $\mu\text{m}$  absorption band is substantially weaker if the pulse is centered on the long-wavelength side of the band. Indeed, the Stokes hump escapes out of the band and prevents absorption [Fig. 2(b), red solid curve, and Fig. 3(b), red dots at  $\lambda_0 \approx 2.9 \mu\text{m}$ ]. A similar absorption asymmetry was identified around the H<sub>2</sub>O molecular band centered at 1.35  $\mu\text{m}$ . The 8-mJ, 96-fs pulse propagated along a 7 m path in air with water vapor (Fig. 4). The nonlinear absorption asymmetry obtained in water vapor reproduces qualitatively the one in air [cf. Figs. 3(b) and 4(b)]. Thus, the nonlinearly enhanced absorption of an ultraintense femtosecond pulse in the vicinity of the natural bands of a gaseous medium appears as a universal phenomenon for selectively absorbing substances.

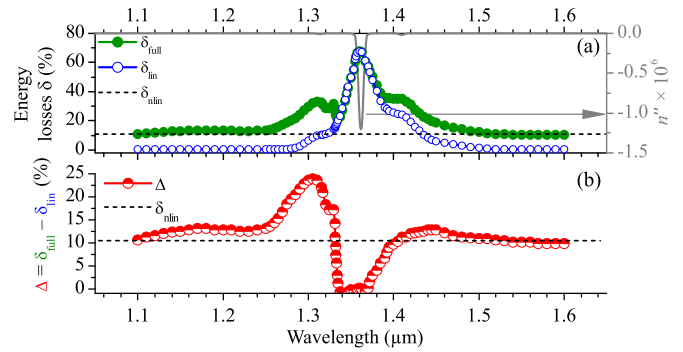


FIG. 4. Same as Figs. 3(a) and 3(b) for the 8 mJ, 96 fs Gaussian pulse with 86 central wavelengths from 1.1 to 1.6  $\mu\text{m}$  and humidity of 100% at 306 K. The power of  $4P_{\text{cr}}$  in the band center (1.35  $\mu\text{m}$ ) has the same excess over critical power as in the 2.7- $\mu\text{m}$  case. The beam diameter of 2 mm was chosen so as to keep the same propagation path of 7 m. The “linear regime” (open circles) corresponds to a pulse energy of 0.01 mJ.

#### IV. ROLE OF DELAYED NONLINEARITY

For all the atmospheric lines studied, the source of the nonlinearly enhanced linear absorption is the systematic downshift of the pulse spectrum and formation of the Stokes hump, where the energy is efficiently transferred from the pump. One possible origin of this downshift is Raman cubic response of rotational transitions in O<sub>2</sub> and N<sub>2</sub> molecules [42]. Rotational excitation may absorb nonresonantly a significant fraction of the initial pulse energy comparable to the ionization losses [45]. To explicitly separate the fraction of energy extracted from a femtosecond pulse to twist the diatomic air molecules, we propagate our 96-fs, 34-mJ pulse centered in the range 2.2–3.2  $\mu\text{m}$  in air with  $\chi_{\text{rot}}^{(3)} = 0$  in Eq. (3) (“no Raman” conditions). The absorption due to rotational transitions is a noticeable (maximum 3% at 2.65  $\mu\text{m}$ ) but not decisive contribution to the overall absorption on a 7-m path [Fig. 5(a), cf. filled circles and squares]. Moreover, the formation of the separated spectral structure, called by us the Stokes hump, is preserved even without inclusion of the rotational Raman response of molecular oxygen and nitrogen in the simulations [Fig. 5(b)]. Apparently, in the 2.95- $\mu\text{m}$  pulse spectrum, the energy transferred to the Stokes hump is 37% of the initial pulse energy if the rotational transitions are active in our

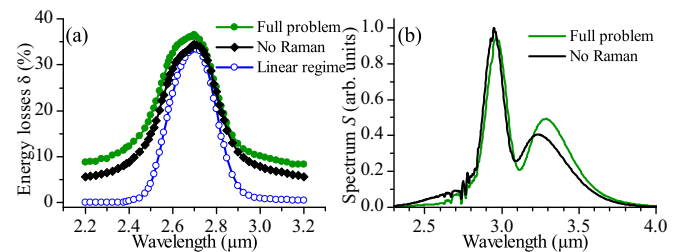


FIG. 5. Contribution of nonlinear excitation of rotational levels: (a) Comparison of net losses in the case of (filled circles) “full problem”, (squares) “no Raman” case, and (open circles) “linear regime”. (b) Spectra of 2.95- $\mu\text{m}$  pulse after filamentation simulated with (green) full model and (black) rotational response turned off.

simulations or 32% with zero delayed nonlinearity. Our results on the Stokes hump formation in instantaneous Kerr media agree with earlier experiments, where such a spectral structure was observed in argon, i.e., an atomic medium without any possibility to excite rotational Raman transitions [27,46].

The physical reason for this hump is self-phase modulation. In the medium with just instantaneous third-order nonlinearity, without diffraction, dispersion, and plasma, the spectrum of a Gaussian pulse splits into two symmetrical maxima: the low- and the high-frequency ones in the front and the rear edges of the pulse, respectively [47]. Free electron generation destroys the trailing edge of the pulse while preserving the leading one. In a bulk medium with weak dispersion, where spatial effects come into play, the high-intensity part of the pulse undergoes redshift and self-focusing simultaneously. Therefore, the redshifted local maximum remains on the beam axis [31].

## V. CONCLUSIONS

In conclusion, we have introduced the concept of a nonlinear transparency window for a high-peak-power mid-infrared pulse propagating in air. We demonstrated that this trans-

parency window exists between 3.1 and 3.5  $\mu\text{m}$  by a diligent scan of the pulse central wavelength in the range 2.2–4.7  $\mu\text{m}$  with a best resolution of 5 nm. We have found the asymmetric character of the nonlinearly enhanced linear absorption of ultraintense femtosecond pulses in the vicinity of atmospheric molecular bands. Due to the Stokes hump formation, the pulse centered at the long-wavelength side of the absorption band within the nonlinear transparency window is the best candidate for the optimum driver wavelength for filament-assisted remote applications. Finally, the asymmetry of the ultraintense pulse losses is found to be a universal phenomenon for selectively absorbing media, and we have shown it for the 1.35- $\mu\text{m}$  water band.

## ACKNOWLEDGMENTS

We thank S. L. Chin, S. V. Chekalin, and V. O. Kompanets for fruitful discussions. This work was supported by the Russian Science Foundation (18-12-00422). W.L. acknowledges support from National Key Research and Development Program (2018YFB0504400) and 111 Project (B16027). P.G.P. acknowledges support from the U.S. AFOSR under MURI Award No. FA9550-16-1-0013.

- 
- [1] D. Strickland and G. Mourou, *Opt. Commun.* **55**, 447 (1985).
- [2] A. Braun, G. Korn, X. Liu, D. Du, J. Squier, and G. Mourou, *Opt. Lett.* **20**, 73 (1995).
- [3] S. L. Chin, S. A. Hosseini, W. Liu, Q. Luo, F. Théberge, N. Aközbeke, A. Becker, V. P. Kandidov, O. G. Kosareva, and H. Schroeder, *Can. J. Phys.* **83**, 863 (2005).
- [4] V. P. Kandidov, S. A. Shlenov, and O. G. Kosareva, *Quantum Electron.* **39**, 205 (2009).
- [5] A. Couairon and A. Mysyrowicz, *Phys. Rep.* **441**, 47 (2007).
- [6] L. Bergé, S. Skupin, R. Nuter, J. Kasparian, and J.-P. Wolf, *Rep. Prog. Phys.* **70**, 1633 (2007).
- [7] S. L. Chin, T. Wang, C. Marceau, J. Wu, J. Liu, O. Kosareva, N. Panov, Y. Chen, J. Daigle, S. Yuan *et al.*, *Laser Phys.* **22**, 1 (2012).
- [8] A. V. Mitrofanov, A. A. Voronin, D. A. Sidorov-Biryukov, A. Pugžlys, E. A. Stepanov, G. Andriukaitis, S. Ališauskas, T. Flöry, A. B. Fedotov, A. Baltuška *et al.*, *Sci. Rep.* **5**, 8368 (2015).
- [9] Y.-H. Chen, S. Varma, I. Alexeev, and H. Milchberg, *Opt. Express* **15**, 7458 (2007).
- [10] J. K. Wahlstrand, N. Jhajj, E. W. Rosenthal, S. Zahedpour, and H. M. Milchberg, *Opt. Lett.* **39**, 1290 (2014).
- [11] L. Rothman, I. Gordon, Y. Babikov, A. Barbe, D. Chris Benner, P. F. Bernath, M. Birk, L. Bizzocchi, V. Boudon, L. R. Brown *et al.*, *J. Quantum Spectrosc. Radiat. Transfer* **130**, 4 (2013), HITRAN2012 special issue.
- [12] J. Kasparian, M. Rodríguez, G. Méjean, J. Yu, E. Salmon, H. Wille, R. Bourayou, S. Frey, Y.-B. André, A. Mysyrowicz *et al.*, *Science* **301**, 61 (2003).
- [13] M. Rodriguez, R. Bourayou, G. Méjean, J. Kasparian, J. Yu, E. Salmon, A. Scholz, B. Stecklum, J. Eislöffel, U. Laux *et al.*, *Phys. Rev. E* **69**, 036607 (2004).
- [14] H. Wille, M. Rodríguez, J. Kasparian, D. Mondelain, J. Yu, A. Mysyrowicz, R. Sauerbrey, J.-P. Wolf, and L. Woeste, *Eur. Phys. J. Appl. Phys.* **20**, 183 (2002).
- [15] F. Théberge, M. Châteauneuf, V. Ross, P. Mathieu, and J. Dubois, *Opt. Lett.* **33**, 2515 (2008).
- [16] V. Shumakova, S. Ališauskas, P. Malevich, C. Gollner, A. Baltuška, D. Kartashov, A. M. Zheltikov, A. V. Mitrofanov, A. A. Voronin, D. A. Sidorov-Biryukov *et al.*, *Opt. Lett.* **43**, 2185 (2018).
- [17] S. Tochitsky, E. Welch, M. Polyanskiy, I. Pogorelsky, P. Panagiotopoulos, M. Kolesik, E. M. Wright, S. W. Koch, J. V. Moloney, J. Pigeon *et al.*, *Nat. Photon.* **13**, 41 (2019).
- [18] R. Butkus, R. Danielius, A. Dubietis, A. Piskarskas, and A. Stabinis, *Appl. Phys. B* **79**, 693 (2004).
- [19] H. Liang, D. L. Weerawarne, P. Krogen, R. I. Grynko, C.-J. Lai, B. Shim, F. X. Kärtner, and K.-H. Hong, *Optica* **3**, 678 (2016).
- [20] K. Zhao, H. Zhong, P. Yuan, G. Xie, J. Wang, J. Ma, and L. Qian, *Opt. Lett.* **38**, 2159 (2013).
- [21] Y. Fu, B. Xue, K. Midorikawa, and E. J. Takahashi, *Appl. Phys. Lett.* **112**, 241105 (2018).
- [22] D. Kartashov, S. Ališauskas, A. Pugžlys, A. A. Voronin, A. M. Zheltikov, and A. Baltuška, *Opt. Lett.* **37**, 2268 (2012).
- [23] A. V. Mitrofanov, A. A. Voronin, S. I. Mitryukovskiy, D. A. Sidorov-Biryukov, A. Pugžlys, G. Andriukaitis, T. Flöry, E. A. Stepanov, A. B. Fedotov, A. Baltuška *et al.*, *Opt. Lett.* **40**, 2068 (2015).
- [24] P. Panagiotopoulos, P. Whalen, M. Kolesik, and J. V. Moloney, *Nat. Photon.* **9**, 543 (2015).
- [25] N. A. Panov, D. E. Shipilo, V. A. Andreeva, O. G. Kosareva, A. M. Saletsky, H. Xu, and P. Polynkin, *Phys. Rev. A* **94**, 041801(R) (2016).
- [26] E. Nibbering, P. Curley, G. Grillon, B. Prade, M. Franco, F. Salin, and A. Mysyrowicz, *Opt. Lett.* **21**, 62 (1996).

- [27] Y. Chen, F. Théberge, C. Marceau, H. Xu, N. Aközbeek, O. Kosareva, and S. L. Chin, *Appl. Phys. B* **91**, 219 (2008).
- [28] J.-F. Daigle, A. Jaroń-Becker, S. Hosseini, T.-J. Wang, Y. Kamali, G. Roy, A. Becker, and S. L. Chin, *Phys. Rev. A* **82**, 023405 (2010).
- [29] D. Kartashov, S. Ališauskas, A. Pugžlys, A. Voronin, A. Zheltikov, M. Petrarca, P. Bejot, J. Kasparian, J.-P. Wolf, and A. Baltuška, *Opt. Lett.* **38**, 3194 (2013).
- [30] D. Uryupina, N. Panov, M. Kurilova, A. Mazhorova, R. Volkov, S. Gorgutsa, O. Kosareva, and A. Savel'ev, *Appl. Phys. B* **110**, 123 (2013).
- [31] N. A. Panov, D. E. Shipilo, V. A. Andreeva, D. S. Uryupina, A. B. Savel'ev, O. G. Kosareva, and S. L. Chin, *Appl. Phys. B* **120**, 383 (2015).
- [32] L. Bergé, C.-L. Soulez, C. Köhler, and S. Skupin, *Appl. Phys. B* **103**, 563 (2011).
- [33] M. Kolesik, J. M. Brown, A. Teleki, P. Jakobsen, J. V. Moloney, and E. M. Wright, *Optica* **1**, 323 (2014).
- [34] S. V. Chekalin, A. E. Dokukina, A. E. Dormidonov, V. O. Kompanets, E. O. Smetanina, and V. P. Kandidov, *J. Phys. B* **48**, 094008 (2015).
- [35] P. Panagiotopoulos, K. Schuh, M. Kolesik, and J. V. Moloney, *J. Opt. Soc. Am. B* **33**, 2154 (2016).
- [36] K. Schuh, P. Panagiotopoulos, M. Kolesik, S. W. Koch, and J. V. Moloney, *Opt. Lett.* **42**, 3722 (2017).
- [37] Y. E. Geints and A. A. Zemlyanov, *Appl. Opt.* **56**, 1397 (2017).
- [38] A. V. Husakou and J. Herrmann, *Phys. Rev. Lett.* **87**, 203901 (2001).
- [39] M. Kolesik and J. V. Moloney, *Phys. Rev. E* **70**, 036604 (2004).
- [40] R. J. Mathar, *Appl. Opt.* **43**, 928 (2004).
- [41] P. A. Oleinikov and V. T. Platonenko, *Laser Phys.* **3**, 618 (1993).
- [42] E. Nibbering, G. Grillon, M. A. Franco, B. S. Prade, and A. Mysyrowicz, *J. Opt. Soc. Am. B* **14**, 650 (1997).
- [43] J. P. Palastro, T. M. Antonsen, and H. M. Milchberg, *Phys. Rev. A* **86**, 033834 (2012).
- [44] J. M. Brown, A. Couairon, and M. B. Gaarde, *Phys. Rev. A* **97**, 063421 (2018).
- [45] S. Zahedpour, J. K. Wahlstrand, and H. M. Milchberg, *Phys. Rev. Lett.* **112**, 143601 (2014).
- [46] K. F. Mak, J. C. Travers, P. Hölzer, N. Y. Joly, and P. S. J. Russell, *Opt. Express* **21**, 10942 (2013).
- [47] S. A. Akhmanov, V. A. Vysloukh, and A. S. Chirkin, *Optics of Femtosecond Laser Pulses* (AIP, New York, 1992).